Molecular Biology of the Cell
Vol. 20, 1520–1532, March 1, 2009

A Fluorescently Tagged C-Terminal Fragment of p47^{phox} Detects NADPH Oxidase Dynamics during Phagocytosis

Xing Jun Li,* Wei Tian,* Natalie D. Stull,* Sergio Grinstein,† Simon Atkinson,‡ and Mary C. Dinauer*§‖

*Department of Pediatrics (Hematology/Oncology), Herman B Wells Center for Pediatric Research, Riley Hospital for Children, and Departments of §Microbiology/Immunology, ‖Medical and Molecular Genetics, and ‡Medicine (Nephrology), Indiana University School of Medicine, Indianapolis, IN 46202; and †Division of Cell Biology, Hospital for Sick Children, Toronto, Ontario M5G 1X8, Canada

Submitted June 19, 2008; Revised November 7, 2008; Accepted December 24, 2008
Monitoring Editor: Jennifer Lippincott-Schwartz

The assembly of cytosolic p47^{phox} and p67^{phox} with flavocytochrome b_{558} at the membrane is crucial for activating the leukocyte NADPH oxidase that generates superoxide for microbial killing. p47^{phox} and p67^{phox} are linked via a high-affinity, tail-to-tail interaction involving a proline-rich region (PRR) and a C-terminal SH3 domain (SH3b), respectively, in their C-termini. This interaction mediates p67^{phox} translocation in neutrophils, but is not required for oxidase activity in model systems. Here we examined phagocytosis-induced NADPH oxidase assembly, showing the sequential recruitment of YFP-tagged p67^{phox} to the phagosomal cup, and, after phagosome internalization, a probe for PI(3)P followed by a YFP-tagged fragment derived from the p47^{phox} PRR. This fragment was recruited in a flavocytochrome b_{558}-dependent, p67^{phox}-specific, and PI(3)P-independent manner. These findings indicate that p47PRR fragment probes the status of the p67^{phox} SH3b domain and suggest that the p47^{phox}/p67^{phox} tail-to-tail interaction is disrupted after oxidase assembly such that the p67^{phox}-SH3b domain becomes accessible. Superoxide generation was sustained within phagosomes, indicating that this change does not correlate with loss of enzyme activity. This study defines a sequence of events during phagocytosis-induced NADPH oxidase assembly and provides experimental evidence that intermolecular interactions within this complex are dynamic and modulated after assembly on phagosomes.

INTRODUCTION

The superoxide-generating NADPH oxidase of phagocytic leukocytes plays an important role in innate host defense (Vignais, 2002; Dinauer, 2003). This enzyme consists of a membrane-bound flavocytochrome b_{558}, the cytosolic subunits p47^{phox}, p67^{phox}, and p40^{phox} (*phox* for phagocytic oxidase), and the small GTPase Rac2 (Vignais, 2002; Nauseef, 2004; Groemping and Rittinger, 2005). Flavocytochrome b_{558} is the redox center of the enzyme and is composed of two integral membrane proteins, p22^{phox} and gp91^{phox}. Upon cellular activation, p47^{phox}, p67^{phox}, p40^{phox}, and Rac2 translocate from the cytosol to flavocytochrome b_{558}, activating electron transfer from NADPH to O_2 (Vignais, 2002; Groemping and Rittinger, 2005). Genetic defects leading to absence or dysfunction of flavocytochrome b_{558}, p47^{phox} or p67^{phox} result in chronic granulomatous disease (CGD), an inherited immunodeficiency characterized by loss of NADPH oxidase activity, recurrent bacterial and fungal infections, and abnormal inflammatory responses (Dinauer, 2003).

The cytosolic *phox* subunits contain modular domains for protein and lipid binding that mediate key steps in the assembly and activation of the NADPH oxidase complex (see Figure 1A). The p47^{phox} subunit plays a crucial role in organizing oxidase assembly. p47^{phox} contains a PX (*Phox* homology) domain at its N-terminus, followed by two tandemly arranged Src homology 3 (SH3) domains that target a proline-rich region (PRR) in the p22^{phox} subunit of flavocytochrome *b*, an auto-inhibitory region (AIR) that masks the SH3 domains in the resting state, and, at its C-terminus, a PRR that binds with high affinity to the C-terminal SH3b domain of p67^{phox} (Finan *et al.*, 1994; Leto *et al.*, 1994; Leusen *et al.*, 1995; de Mendez *et al.*, 1996; Morozov *et al.*, 1998; Vignais, 2002; Nauseef, 2004; Groemping and Rittinger, 2005; Mizuki *et al.*, 2005). In addition to the SH3b domain, the p67^{phox} subunit contains an N-terminal tetratricopeptide repeat (TPR) region that is a target of Rac-GTP in the assembled oxidase complex, an activation domain that regulates electron transfer through the flavocytochrome *b*, a second SH3 domain of uncertain function, and a PB1 (*Phox* and Bem1) motif that binds to a complementary PB1 domain in p40^{phox} (Figure 1A; Ito *et al.*, 2001; Vignais, 2002; Nauseef, 2004; Groemping and Rittinger, 2005). The role of the p40^{phox}

This article was published online ahead of print in *MBC in Press* (http://www.molbiolcell.org/cgi/doi/10.1091/mbc.E08–06–0620) on January 7, 2009.

Address correspondence to: Mary C. Dinauer (mdinauer@iupui.edu).

Author contributions: X.J.L. designed, performed and analyzed experiments, prepared the figures, and drafted the manuscript. W.T. helped to set up the live imaging system for analysis of NADPH oxidase assembly during phagocytosis, N.S. helped with retrovirus transductions in PLB-985 cells, and S.G. and S.A. helped with experimental design and interpretation of the data. M.C.D. oversaw this entire project including the experimental design, analysis, and interpretation of the data, and preparation of the manuscript.

Abbreviations used: aa, amino acid; CGD, chronic granulomatous disease; DCF, dichlorodihydrofluorescein; IgG-Zym, IgG-opsonized zymosan; O_2^-, superoxide; PB1, *Phox* and Bem1; PI(3)P, phosphatidylinositol 3-phosphate; PRR, proline-rich region; PX, PhoX domain; SH3, Src homology 3; SOD, superoxide dismutase.

subunit has been poorly understood, and mutations in its corresponding gene are not a cause of CGD. However, recent studies showed that p40^{phox} stimulates phagocytosis-induced NADPH oxidase activity via PI(3)P (phosphatidylinositol 3-phosphate), a phosphoinositide that accumulates on internalized phagosomes and binds to a PX domain at the p40^{phox} N-terminus (Ellson *et al.*, 2006a, b; Suh *et al.*, 2006; Tian *et al.*, 2008).

In unstimulated neutrophils, the three cytosolic *phox* proteins can be isolated from neutrophils as a heterotrimeric complex with a 1:1:1 stoichiometry, which is formed by the "tail-to-tail" SH3b-PRR association between p67^{phox} and p47^{phox}, and the PB1-PB1 interaction between p67^{phox} and p40^{phox} (Figure 1A; Lapouge *et al.*, 2002; Groemping and Rittinger, 2005). A recent study suggested that although p67^{phox} and p40^{phox} are associated constitutively in unstimulated neutrophils, the tail-to-tail interaction between p67^{phox} and p47^{phox} is formed as an early event in neutrophil activation (Brown *et al.*, 2003). Translocation of the heterotrimeric complex to flavocytochrome *b* is driven by activation-induced serine phosphorylation of the p47^{phox} AIR, resulting in unmasking of the tandem SH3 domains in p47^{phox} for binding to p22^{phox} (Leto *et al.*, 1994; Sumimoto *et al.*, 1996; Groemping *et al.*, 2003). The interaction between p47^{phox} and p22^{phox} is essential for the recruitment of the p47^{phox}/p67^{phox}/p40^{phox} complex to the flavocytochrome *b* (el Benna *et al.*, 1994; Fontayne *et al.*, 2002; Vignais, 2002; Nauseef, 2004; Groemping and Rittinger, 2005). Evidence for this is provided by the observation that neither p67^{phox} nor p40^{phox} are able to firmly translocate to membranes in chronic granulomatous disease neutrophils lacking flavocytochrome *b* or p47^{phox} (Heyworth *et al.*, 1991; Dusi *et al.*, 1996; Allen *et al.*, 1999) or when there are mutations in the proline-rich region of p22^{phox} that disrupt binding to p47^{phox} (Nauseef, 2004; Groemping and Rittinger, 2005). Of interest, C-terminal truncations of p67^{phox}, which lack the SH3b domain and therefore lack the tail-to-tail interaction with p47^{phox}, are active in cell-free systems and in whole cells exhibit spontaneous translocation and support partial NADPH oxidase activity (de Mendez *et al.*, 1994; Leusen *et al.*, 1995; de Mendez *et al.*, 1996; Hata *et al.*, 1998; Arias *et al.*, 2004). Taken together, these observations suggest that although the tail-to-tail association between p47^{phox} and p67^{phox} plays a crucial role in organizing oxidase assembly under physiological conditions, this association may not be required for NADPH oxidase activity after assembly of the holoenzyme.

Although much has been learned about the interactions between different NADPH oxidase subunits that contribute to formation of the enzyme complex, relatively little is known about whether these undergo subsequent alteration after enzyme assembly. Imaging of fluorescently tagged proteins is a useful modality for analyzing temporal and spatial events during phagocytosis, which we applied in this study to investigate the dynamics of NADPH oxidase assembly and the p47^{phox}/p67^{phox} tail-to-tail interaction. We developed a yellow fluorescent protein (YFP)-tagged probe derived from the C-terminal PRR of p47^{phox} and monitored its cellular location by confocal videomicroscopy in neutrophil-differentiated PLB-985 cells stimulated with IgG-opsonized zymosan (IgG-Zym). We observed that YFP-p47PRR accumulated on internalized IgG-Zym phagosomes in a flavocytochrome b_{558}-dependent and p67^{phox}-specific manner after, although independent of, the accumulation of PI(3)P. This result indicates that the tail-to-tail association between p47^{phox} and p67^{phox} must be disrupted after membrane translocation in order to allow p47PRR access to the p67^{phox} SH3b domain. Thus, the fluorescence-tagged p47PRR fragment acts as a probe that reveals changes in the interaction between two regulatory NADPH oxidase subunits after enzyme assembly on the phagosome.

MATERIALS AND METHODS

Reagents and Antibodies

Chemicals were purchased from Sigma-Aldrich (St. Louis, MO) unless otherwise stated. PBS, pH 7.2, penicillin/streptomycin, neomycin, trypsin/EDTA, Lipofectamine Plus reagent, DMEM with low glucose, and RPMI 1640 were from Invitrogen Invitrogen (Carlsbad, CA), and bovine growth serum and FCS were from Hyclone Laboratory (Logan, UT). Glutathione-Sepharose-4B was purchased from Amersham Biosciences (Piscataway, NJ). Fc OxyBURST Green (F2902) was purchased from Invitrogen. G418 from Calbiochem (San Diego, CA) and ECL detection kit from Pierce (Rockford, IL). Polyclonal antibody against green fluorescent protein (GFP) was obtained from Santa Cruz Biotechnology (Santa Cruz, CA). Rabbit polyclonal antibody against p40^{phox} was from Upstate Biotechnology (Lake Placid, NY), and monoclonal antibodies against p67^{phox} and p47^{phox}, respectively, was from BD Biosciences (Franklin Lakes, NJ).

Plasmid Constructions

The DNA fragment encoding p47PRR (355–390 amino acids of p47^{phox}) was amplified from pRK5-p47^{phox} (gift from Dr. Lambeth, Emory University Medical School, Atlanta, GA) by PCR and cloned into EcoRI and KpnI sites of pEYFP-C1 (BD Biosciences Clontech, San Diego, CA) to generate pEYFP-p47PRR. Site-directed mutagenesis of p47PRR was performed in pEYFP-p47PRR using the QuikChange Site-Directed Mutagenesis kit (Stratagene, La Jolla, CA). The p47PRR cDNA with flanking EcoRI and KpnI restriction sites was ligated to the mCherry cDNA(Shaner *et al.*, 2004; gift from R. Tsien, University of California at San Diego) by insertion into a pEYFP-C1-based plasmid (gift from J. Swanson, University of Michigan) in which the EYFP cDNA had been replaced with that of mCherry. Flanking HpaI and ClaI restriction sites were placed on the YFP-p47PRR cDNA by PCR for ligation into the pMSCVpuro vector (BD Clontech), in which the puromycin resistance cassette was removed. YFP-tagged p40PX cDNA was digested with AgeI from pEYFP-p40PX,(Suh *et al.*, 2006) blunted, digested with EcoRI, and subcloned into the HpaI and EcoRI sites of pMSCVpuro, and the puromycin resistance cassette was then removed by digesting with EcoRI and ClaI, blunting, and relegating. A cDNA encoding the p40^{phox} PX domain with flanking EcoRI and KpnI restriction sites was generated by PCR from the pEYFP-C1 plasmid containing YFP-p40PX, which was ligated to the mCherry plasmid derived from pEYFP-C1 described above. The pMSCV-mCherry-p40PX plasmid was obtained by using the same strategy as for the generation of pMSCV-YFPp40PX. All the constructs were confirmed by sequencing.

Cells

COS-7 cells were grown in low-glucose DMEM with 10% bovine growth serum at 37°C under 5% CO_2.(Price *et al.*, 2002; Suh *et al.*, 2006). Lipofectamine Plus reagent (Invitrogen) was used to transiently transfect 4 μg plasmid DNA per 100-mm plate of COS-7 cells. Cells were generally analyzed 24 h after transfection (Price *et al.*, 2002; Ming *et al.*, 2007).

Human PLB-985 myelomonocytic cells or X-CGD PLB-985 cells with a targeted disruption of the gp91^{phox} gene were cultured as described previously (Zhen *et al.*, 1993; Li *et al.*, 2005). Amaxa kit V (Amaxa Biosystems, Cologne, Germany) was used to transfect plasmids according to the manufacturer's instructions. Briefly, 2×10^6 PLB-985 cells were resuspended in 100 μl Amaxa solution V, followed by adding 2 μg pEYFP-p47PRR or pEYFP-p47PRR mutant, and electroporated using the Amaxa program C-23 (Amaxa Biosystems). Clones were selected by limiting dilution in the presence of 1.5 mg/ml G418 for 3-4 wk (Li *et al.*, 2005). YFP-positive clones were identified by flow cytometry and maintained in 0.5 mg/ml G418. PLB-985 cells with stable expression of p67^{phox}-YFP, or YFP-p40PX, or mCherry-p40PX were generated by retroviral transduction with VSVG-pseudotyped MSCV-p67^{phox}-YFP, MSCV-YFP-p40PX, or MSCV-mCherry-p40PX packaged using the Pantropic Retroviral Expression System (BD Clontech; Suh *et al.*, 2006). X-CGD PLB-985 cells with stable expression of p67^{phox}-YFP or YFP-p47PRR were generated by retroviral transduction with VSVG-pseudotyped MSCV-p67^{phox}-YFP or MSCV-YFP-p47PRR. After transduction, YFP-positive cells were isolated by cell sorting (FACSCalibur, Becton Dickinson, San Diego, CA). PLB-985 cells expressing either p67^{phox}-YFP or YFP-p47PRR were transduced with pMSCV-mCherry-p40PX and selected for mCherry expression using PE-Texas Red laser (BD FACSAria, Becton Dickinson). For neutrophil differentiation, PLB-985 cells were cultured in 0.5% dimethylformamide (DMF) for 5-6 d (Zhen *et al.*, 1993; Li *et al.*, 2005).

Glutathione S-transferase-p67^{phox} Fusion Protein-binding Assay

In vitro binding assays were performed as described previously with little modification (Ming *et al.*, 2007). Ten micrograms cell lysate from transiently transfected COS-7 cells was incubated with 0.1 nmol of immobilized gluta-

thione *S*-transferase (GST)-p67^{phox} in binding buffer (50 mM Tris-HCl, pH 7.4, 1% Triton X-100, 150 mM NaCl, 2 mM EDTA, 20 μg/ml chymostatin, 2 mM phenylmethylsulfonyl fluoride [PMSF], 10 μM leupeptin, and 1 mM 4-(2-aminoethyl) benzenesulfonyl fluoride [AEBSF]; Ming *et al.*, 2007) for 60 min at 4°C with end-to-end rotation. After incubation, the glutathione-Sepharose beads were extensively washing with binding buffer, and bound proteins were subjected to SDS-PAGE and detected by immunoblotting with anti-GFP polyclonal Ab, which also recognizes YFP, and visualized with ECL detection as previously described (Price *et al.*, 2002; Suh *et al.*, 2006).

Preparation of IgG-opsonized Zymosan

Zymosan (zymosan A from *Saccharomyces cerevisiae*, Sigma, Z-4250) was opsonized with zymosan A Bioparticles opsonizing reagent (Molecular Probes, Eugene, OR; Z-2850, Invitrogen), which is rabbit polyclonal IgG antibody specific for the zymosan particles, according to the manufacturer's instructions with slight modification. Briefly, zymosan A particles were resuspended in 0.9% NaCl at the concentration of 20 mg/ml and heated at 100°C for 15 min. After extensively washing with PBS, zymosan particles were sonicated three times for 5 s to disperse aggregates. Zymosan A particles were then opsonized with zymosan A Bioparticles opsonizing reagent at 37°C with end-to-end rotation for 60 min, followed by extensive washing and sonication. IgG-Zym particles were resuspended in PBS at 20 mg/ml and stored at −20°C until using. In some studies (immunostaining of p47^{phox}, diphenylene iodonium [DPI] inhibitor studies), human IgG was used to opsonize zymosan.

Immunoblotting and Densitometry Analysis of phox Subunit Expression

Neutrophil-differentiated PLB-985 cell lysates were prepared for electrophoresis and Western blots performed as described previously (Zhen *et al.*, 1993; Price *et al.*, 2002; Li *et al.*, 2005; Suh *et al.*, 2006; Ming *et al.*, 2007). Image J (NIH, free software; http://rsb.info.nih.gov/ij/) was used for densitometry analysis.

Activation of the NADPH Oxidase in Intact Cells

Superoxide production was measured by chemiluminescence as described previously (Dahlgren and Karlsson, 1999; Li *et al.*, 2002; Ming *et al.*, 2007). Briefly, 5×10^5 neutrophil-differentiated PLB-985 cells in PBSG (PBS plus 0.9 mM $CaCl_2$, 0.5 mM $MgCl_2$, and 20 mM dextrose) in the presence of 20 μM isoluminol and 20 U/ml horseradish peroxidase were prewarmed 10 min at 37°C, and NADPH oxidase activity was initiated by adding 300 ng/ml phorbol 12-myristate acetate (PMA). Luminescence was recorded every 1 min for a total of 30 min at 37°C using an Lmax microplate luminometer (Molecular Devices, Sunnyvale, CA). A similar protocol was used to detect O_2^- production in phagosomes after IgG-Zym (400 μg/ml) activation in the presence of 20 μM luminol, 75 μg/ml superoxide dismutase (SOD), and 2000 U/ml catalase (Dahlgren and Karlsson, 1999) with cells monitored for 60 min. In some experiments, PLB-985 granulocytes expressing p67^{phox}-YFP or YFP-p47PRR were pretreated with 10 μM DPI at 37°C for 15 min, before NADPH oxidase assays. A synchronized phagocytosis assay was used for IgG-Zym–induced NADPH oxidase activity assays (Tian *et al.*, 2008).

Intracellular O_2^- production in cells stimulated with Fc OxyBURST Green (Molecular Probes) was measured in a luminol-based chemiluminescence assay modified from a synchronized phagocytosis assay (Greenberg *et al.*, 1990; DeLeo *et al.*, 1999). Briefly, 5×10^5 neutrophil-differentiated PLB-985-mCherry-p40PX cells in 200 μl PBSG were added to wells of a 96-well plate, and incubated for 5 min on ice, and then 25 μl cold Fc OxyBURST Green particles was added to the cells. The cells and particles were spun down at 1200 rpm for 5 min at 4°C, the PBSG was removed carefully from the wells, and the chemiluminescence assay was initiated by adding prewarmed PBGS containing 20 μM luminol in the presence or absence of 75 μg/ml SOD and 2000 U/ml catalase (Dahlgren and Karlsson, 1999). Phagosomal NADPH oxidase activity during nonsynchronized phagocytosis of Fc OxyBURST Green was also measured using the same protocol as described above for IgG-Zym induced NADPH oxidase activity.

RNA Interference (p40^{phox} Knockdown Assay)

The short-hairpin (sh) RNA primer (5′-GATCCGGGCATCTTCCCTCTCTC-CTTCGTGAATTCAAGAGATTCACGAAGGAGAGAGGGAAGATGCCCTT-TTTG-3′) against the human p40^{phox} coding sequence (^{684}GGGCATCTTC-CCTCTCTCCTTCGTGAA^{711}) was designed using Integrated DNA Technologies online program (Coralville, IA; Tian *et al.*, 2008). shRNA was subcloned into pSuper.neo vector (the pSuper RNAi system, OligoEngine, Seattle, WA) using BglII/HindIII sites. The construct was confirmed by sequencing. For p40^{phox} knockdown, 2×10^6 WT PLB-985 cells, resuspended in 100 μl of solution V (Amaxa Biosystems), were transfected with 2 μg pSuper.neo encoding shRNA using the C-23 program (Amaxa Biosystems). Positive clones were selected by limiting dilution in the presence of 1.8 mg/ml G418. After selection, positive clones were differentiated with 0.5% DMF and tested by Western blotting using anti-p40^{phox} polyclonal Ab (07–503, Upstate Biotechnology). A clone with p40^{phox}-knockdown was transduced with pMSCV-YFP-p47PRR and sorted for YFP expression using a FACSCalibur (Becton Dickinson).

Living Image by Confocal Videomicroscopy

A spinning-disk (CSU10) confocal system mounted on a Nikon TE-2000U inverted microscope (Melville, NY) with an Ixon air-cooled EMCCD camera (Andor Technology, South Windsor, CT) and a Nikon Plan Apo 100× 1.4 NA. objective was used to film phagocytosis in living PLB-985 neutrophils in real time. Neutrophil differentiated PLB-985 cells, 5×10^5, in 150 μl PBSG (Price *et al.*, 2002; Suh *et al.*, 2006) were loaded onto a 35-mm glass-bottom microwell dish (MatTek Cultureware, Ashland, MA; Gamma irradiated, TK0275), which was mounted on the microscope and maintained at 37°C using a stage incubator (Warner Instruments, Hamden, CT). Cells were allowed to adhere for 5 min before 5 μl IgG-Zym particles (20 mg/ml) was added, followed by filming. In some experiments, PLB-985 granulocytes expressing p67^{phox}-YFP or YFP-p47PRR were pretreated with 10 μM DPI or 100 nM wortmannin at 37°C for 15 min, before the phagocytosis assay. Supplementary Movies were made over a ≈30-min interval after addition of the IgG-Zym. Live images were collected in a single confocal plane (1 μm) with 488- and/or 568-nm excitation and 0.3-s exposure with a time lapse of 10 s. A field of cells was typically filmed for a 5–8 min period, after which time for phagosomes often moved into different focal plane. All images were analyzed with Metamorph software (Universal Imaging, Downingtown, PA). Each type of experiment was performed on at least three independent occasions.

Image J (NIH) was used to analyze the accumulation of fluorescent probes on phagosomes relative to their cytoplasmic distribution. An area of the phagosome rim (≈20% of the total rim) was outlined by hand, the mean fluorescence intensity within the area was determined, and ratios were determined against the value from a corresponding area in the cytoplasm close to the phagosome. For each probe analyzed, 5–10 phagosomes for PLB-985 neutrophils monitored at each stage—cup, closure (time of sealing), and postinternalization (150–250 s)—were analyzed with this method, and the mean ± SEM was determined. To analyze the kinetics of probe accumulation, the time to the first appearance of YFP-tagged proteins on the phagosome membrane, relative to the time of phagosome closure, was determined for 18 YFP-positive phagosomes in cells expressing p67^{phox}-YFP, YFP-p40PX, or YFP-p47PRR. Images were collected in at least four independent experiments for each cell line. Statistical analysis was used to determine the difference between groups.

Immunofluorescence Microscopy

Immunostaining of endogenous p47^{phox} was performed after synchronized phagocytosis. Briefly, 2.5×10^6 neutrophil-differentiated PLB-985-p67^{phox}-YFP or X-CGD PLB-985-p67^{phox}-YFP cells in 2 ml PBSG were added to coverslip-bottomed dishes (MatTek Cultureware) and incubated for 5 min on ice before adding 30 μl IgG opsonized zymosan (20 mg/ml). The cells and particles were spun down at 1200 rpm for 5 min at 4°C and then incubated at 37°C for 13 min. Phagocytosis was stopped by putting the cells on ice, which were then washed with cold PBS, fixed with 4% paraformaldehyde for 10 min at room temperature, permeabilized with 0.1% Triton X-100 in PBS, blocked with 10% goat serum plus 2% bovine serum albumin (BSA) in PBS, and immunostained with anti-p47^{phox} followed by Alexa-555 goat anti-mouse IgG1. Cells were imaged on a spinning-disk (CSU10) confocal system mounted on a Nikon TE-2000U inverted microscope with an Ixon air-cooled EMCCD camera (Andor Technology) and a Nikon Plan Apo 100× 1.4 NA. objective. Images shown are representative of at least three independent experiments.

Imaging of Phagocytosis-induced NADPH Oxidase Activity Using Nitroblue Tetrazolium and Fc OxyBURST Green

NADPH oxidase activity in phagosomes was visualized during videomicroscopy using nitroblue tetrazolium (NBT). To facilitate the identification of IgG-Zym particles that were ingested, PLB-985 neutrophils expressing fluorescently tagged p67^{phox} or p47PRR were used. Briefly, 5×10^5 PLB-985 neutrophils expressing fluorescently tagged p67^{phox} or p47PRR in PBSG containing 20% of a saturated NBT solution were incubated at 37°C for 5 min in a 35-mm glass-bottom microwell dish before 5 μl IgG-Zym particles (20 mg/ml) was added. Phagocytosis was recorded on a spinning disk confocal system as above. Brightfield was used to observe the dark purple formazan deposits (Suh *et al.*, 2006).

Visualization of NADPH oxidase activity during phagocytosis was also performed using Fc OxyBURST Green (Ryan *et al.*, 1990), which fluoresces in the presence of H_2O_2. Briefly, 5×10^5 neutrophil-differentiated PLB-985-mCherry-p40PX cells in 150 μl PBSG were loaded in a 35-mm glass-bottom microwell dish and incubated for 5 min at 37°C. Twenty-five microliters Fc OxyBURST Green particles (3 mg/ml) was washed with PBS and resuspended in 25 μl PBSG before adding to the cells. Phagocytosis was recorded on a spinning disk confocal system as previously described. The intensity of dichlorofluorescein (DCF) fluorescence within the phagosome was considered as 1 at the time at which mCherry-p40PX first appeared on internalized phagosomes. Image J software was used to analyze the intensity of phagosomal DCF fluorescence at different time points after the accumulation of mCherry.

RESULTS

In Vitro Interaction of Fluorescently Tagged C-Terminal Fragment of p47phox with Full-Length p67phox

To investigate the stability of the p67*phox*/p47*phox* tail-to-tail interaction, we designed a YFP-tagged probe derived from the C-terminus of p47*phox* (amino acids 355-390; Figure 1A), referred to as YFP-p47PRR, which should detect the SH3b domain of p67*phox*. In initial experiments, we examined whether YFP-p47PRR could bind to full-length GST-tagged p67*phox*. In parallel, we evaluated a series of YFP-p47PRR mutants to assess specificity for the SH3b domain of p67*phox*. On the basis of work done by several groups showing that both the PRR (residues 360–369) and an "extra-PRR" region (residues 370–390) are important for the high-affinity tail-to-tail interaction between p67*phox* and p47*phox* (Kami *et al.*, 2002; Groemping and Rittinger, 2005; Massenet *et al.*, 2005; Mizuki *et al.*, 2005), we focused on prolines at positions 363 and 366, which are components of the core PxxP motif, arginine 368, and two lysines at positions 383 and 385 in the extra-PRR region (numbered according to the location in full-length of p47*phox*; Figure 1A). COS-7 cell–expressed YFP-p47PRR could be pulled down by GST-tagged p67*phox* (Figure 1B), similar to full-length untagged p47*phox* (not shown). As expected, YFP did not bind to GST-p67*phox* (Figure 1, B–D), and GST alone was unable to bind to YFP-p47PRR (not shown). Figure 1D is a summary of three independent assays in which the relative level of bound YFP-p47PRR or mutant derivatives was normalized to expression in the corresponding cell lysate. A P366A mutation in YFP-p47PRR was sufficient to induce a substantial decrease in binding to GST-p67*phox*, with similar results obtained for any of the derivatives harboring this or the other core PxxP mutation, P363A/P366A (Figure 1, B and D), confirming previous studies (de Mendez *et al.*, 1996; Hata *et al.*, 1997; Kami *et al.*, 2002; Groemping and Rittinger, 2005; Massenet *et al.*, 2005; Mizuki *et al.*, 2005). A double K383E/K385E mutation in the extra-PRR region had less effect on binding to GST-p67*phox*, whereas a R368A-K383E/K385E mutant had almost complete loss of interaction in this assay (Figure 1, B and D), consistent with the important contribution of Arg368 in binding to the p67*phox* SH3b domain (Kami *et al.*, 2002). Thus, YFP-p47PRR exhibits binding to full-length p67*phox* in vitro and mutagenesis studies provide support that the SH3b domain of *p67phox* is the target of YFP-p47PRR in this assay.

Generation of Transgenic PLB-985 Cells Expressing YFP-tagged phox Proteins

To examine the behavior of YFP-PRR during phagocytosis, we generated PLB-985 myelomonocytic cells with stable expression of YFP-p47PRR, and, for comparison, YFP alone, YFP-p47PRR-P366A, YFP-p47PRR-K383E/K385E, p67*phox*-YFP, or YFP-p40PX, a YFP-tagged protein derived from the PX domain of p40*phox* that is a sensitive probe for PI(3)P. The level of transgenic protein expression was similar in each of these lines, as assessed by flow cytometry (Figure 2A) and by immunoblot analysis using an anti-GFP polyclonal antibody (Figure 2B). We could not compare the expression level of YFP-p47PRR with that of endogenous p47*phox* because of the unavailability of an anti-p47*phox* antibody with comparable affinity for each. Using an anti-p67*phox* mAb, similar expression levels of p67*phox*-YFP and endogenous p67*phox* were observed in the p67*phox*-YFP transgenic PLB-985 cell line (Supplementary Figure S1), which taken together with Figure 2B, provides indirect evidence that YFP-p47PRR expression was comparable to that of endogenous p67*phox*.

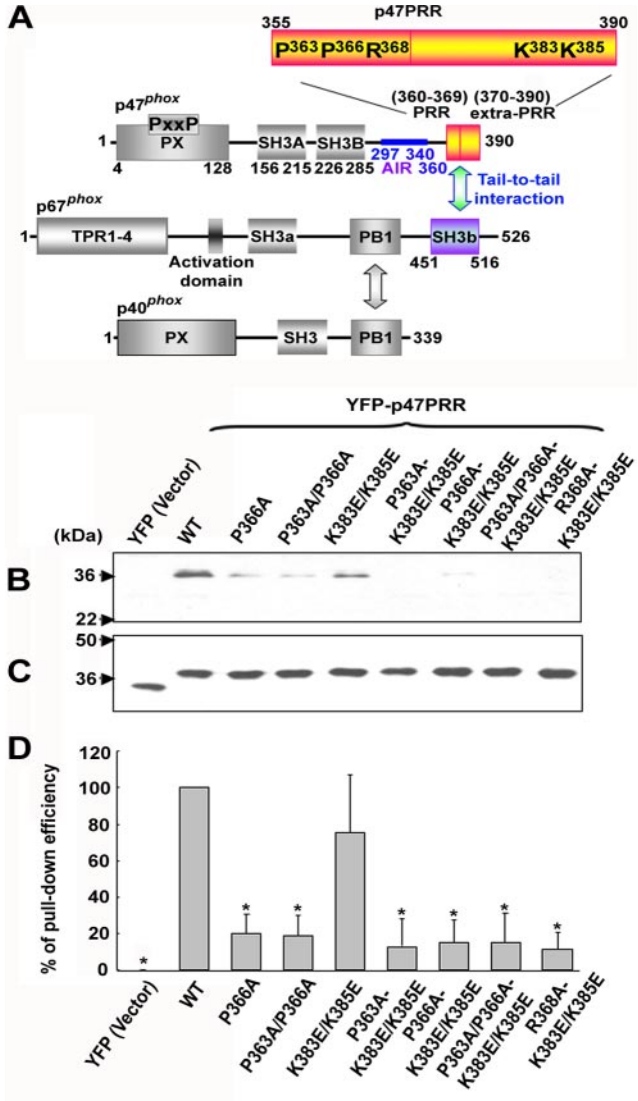

Figure 1. Interactions of p67*phox* with other cytosolic *phox* components and with p47PRR and its mutants in vitro. (A) Structural motifs and the proposed interactions between p47*phox*, p67*phox*, and p40*phox* are shown schematically, in addition to the YFP-tagged C-terminal fragment of p47*phox*, YFP-p47PRR, used in this study. Mutants in the YFP-tagged C-terminal fragment of p47*phox* are also indicated, numbered according to their position in full-length p47*phox*. (B) COS-7 cells were transfected with the empty pEYFP-C1 vector (YFP), pEYFP-C1 encoding p47PRR (YFP-p47PRR) or p47PRR mutants. Ten micrograms of cell lysate was incubated with glutathione-Sepharose-4B–bound GST-p67*phox*, and bound material was electrophoresed and immunoblotted with anti-GFP polyclonal antibody. Blots are representative of three independent experiments. (C) Immunoblot of 10 μg cell lysate, corresponding to samples shown in B. (D) The bar graph shows the relative recovery of GST-p67*phox* -bound YFP-p47PRR and mutant derivatives, relative to the amount present in the lysate, based on densitometry of immunoblots of pulldown samples and cell lysates. The recovery of wild-type YFP-p47PRR considered as 1.0. Assays were performed in triplicate, and mean ± SD are shown. *$p < 0.01$.

NADPH oxidase activity in response to either PMA or IgG-Zym in neutrophil-differentiated PLB-985 cells expressing YFP-tagged proteins was comparable to activity measured in cells expressing YFP alone and to parental PLB-985 cells (Figure 2, C and D, and data not shown). Thus, expression of

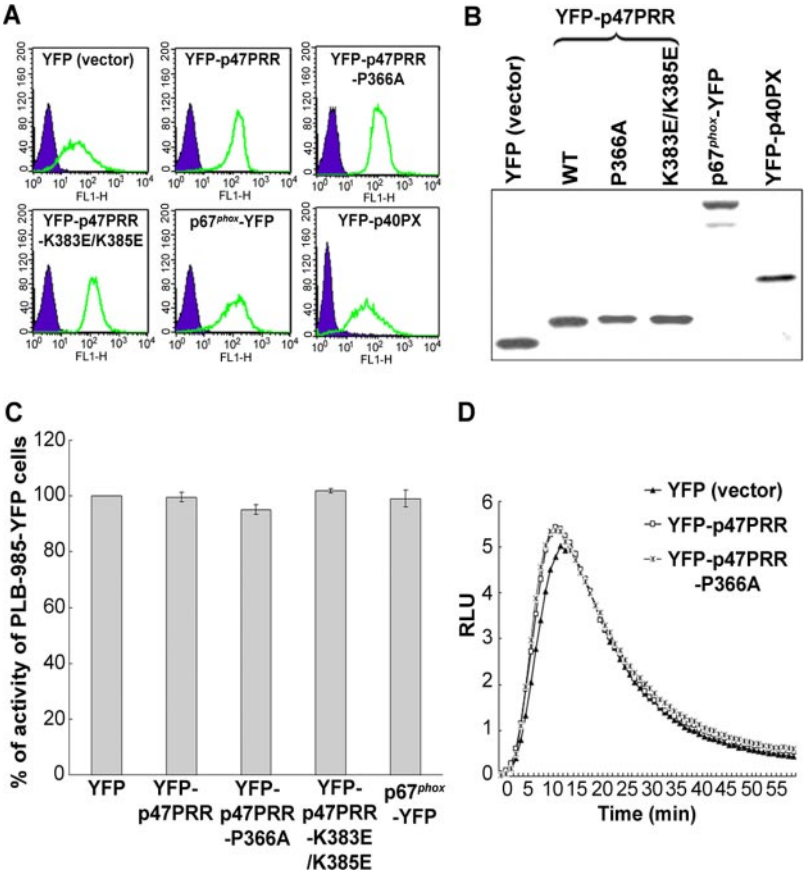

Figure 2. Expression of YFP or YFP-fusion proteins in stably transgenic PLB-985 cells. (A) YFP or YFP-fusion protein expression was measured by flow cytometry. (B) Western blot analysis of YFP or YFP-fusion proteins using anti-GFP polyclonal antibody. (C) PMA-stimulated superoxide production in transgenic PLB-985 neutrophils. Results are expressed as total relative light unit (RLU) value over 30 min, measured at 1-min intervals. Values represent the mean ± SD of triplicate determinations. (D) IgG-Zym–stimulated superoxide production in phagosomes was measured for 60 min in PLB-985 neutrophils expressing empty vector (YFP), or YFP-p47PRR, or YFP-p47PRR-P366A mutant, using SOD-resistant luminol-enhanced chemiluminescence.

YFP-p47PRR or its mutants did not interfere with oxidase activity stimulated by either PMA or IgG-Zym.

Localization of Fluorescent Proteins by Time-Lapse Confocal Videomicroscopy during Phagocytosis of IgG-Zym

To investigate the localization of fluorescent proteins during phagocytosis of IgG-Zym by PLB-985 neutrophils, we used live imaging with confocal videomicroscopy. To validate our methodology, we examined YFP and YFP-tagged full-length p67^{phox} as a negative and a positive control, respectively. In cells expressing YFP alone, fluorescence was distributed in the cytosol and nucleus, and there was no accumulation around IgG-phagosomes (Figure 3, A and B; Supplementary Movie S1), similar to observations in RAW 264.7 macrophages (Ueyama *et al.*, 2007). However, YFP-tagged p67^{phox}, which was cytosolic in resting cells, accumulated on the cup of nascent phagosomes and persisted after sealing, as previously reported (Allen *et al.*, 1999; van Bruggen *et al.*, 2004), being visible for at least for 5 min from the first appearance on the cup (Figure 3, A and B; Supplementary Movie S2). YFP-p40PX, which detects PI(3)P, was distributed in the cytoplasm and on vesicular structures in resting cells. YFP-p40PX was not visible in the phagosomal cup, but accumulated around the phagosome after sealing and internalization (Figure 3A; Supplementary Figure S2 and Supplementary Movie S3), consistent with observations in RAW 264.7 macrophages (Ellson *et al.*, 2001; Vieira *et al.*, 2001). In unstimulated PLB-985 neutrophils, YFP-p47PRR was cytosolic, but also accumulated on phagosomes after sealing and internalization and was detected for at least 5 min after its first appearance (Figure 3, A and B; Supplementary Movie S4). This observation suggests that the SH3b domain of p67^{phox} becomes accessible to the YFP-p47PRR probe after phagosome internalization.

We also examined the kinetics of phagosome formation and the accumulation of p67^{phox}-YFP, YFP-p40PX, and YFP-p47PRR in individual phagosomes relative to the time of phagosomal closure (Figure 3, B and C). The mean time to closure (sealing) from the time the phagosomal cup was first visible was similar for all three transgenic lines: 45 ± 15, 44 ± 10, and 45 ± 22 s ($n \geq 4$) for p67^{phox}-YFP, YFP-p40PX, and YFP-p47PRR, respectively. Accumulation of p67^{phox}-YFP was typically first visible on the phagosomal cup (−29 ± 32 s before sealing, mean ± SD, $n = 18$), whereas the accumulation of YFP-p40PX and of YFP-p47PRR was not observed until 33 ± 23 and 61 ± 20 s after closure, respectively (Figure 3C). The differences in the mean times at which each YFP-tagged protein was first detected on phagosomes were statistically significant for each pair ($p < 0.01$). Thus, these results show that there is sequential recruitment of p67^{phox}-YFP, YFP-p40PX, and YFP-p47PRR to phagosomes, respectively, and that the appearance of YFP-p47PRR lags that of PI(3)P accumulation.

YFP-p47PRR Translocation Is Flavocytochrome b_{558}-dependent and Targets the SH3b Domain of p67^{phox}

We next performed experiments designed to verify that accumulation of the YFP-p47PRR probe on IgG-Zym phagosomes is dependent on flavocytochrome b_{558}, as previously shown for p67^{phox} (Allen *et al.*, 1999; van Bruggen *et al.*, 2004) and that YFP-p47PRR accumulation requires intact binding to the SH3b domain of p67^{phox}. First, X-CGD PLB-985 cells (Zhen *et al.*, 1993), which lack flavocytochrome b_{558} and NADPH oxidase activity, were engineered to express either

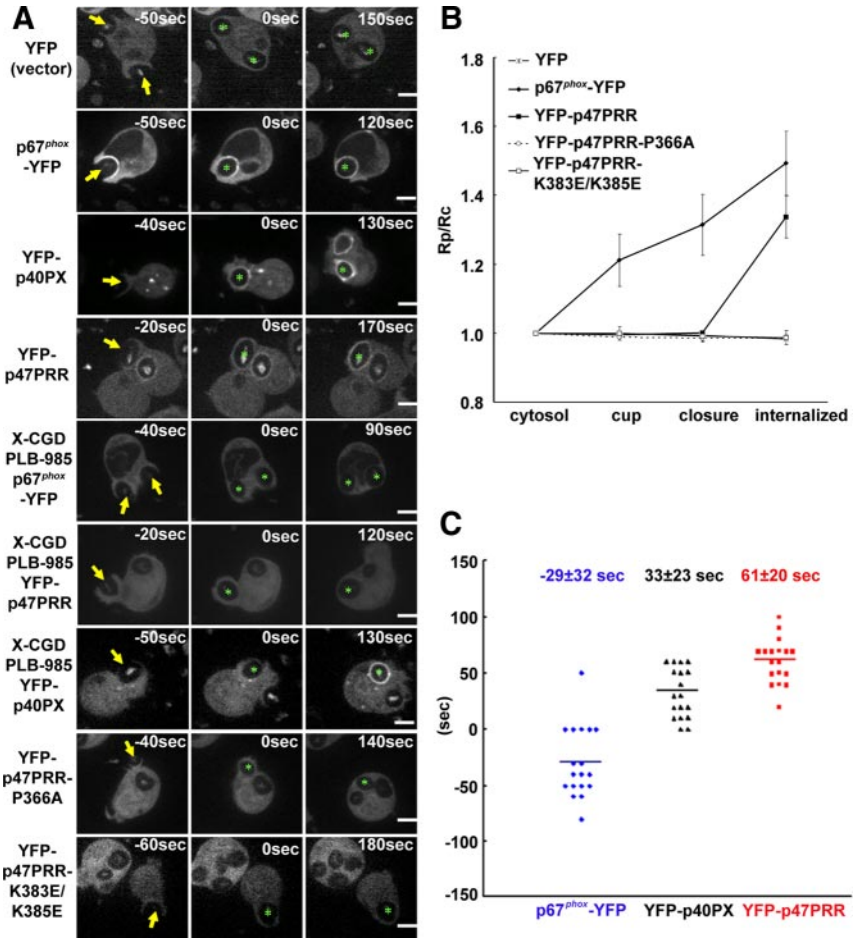

Figure 3. Translocation of fluorescent proteins during IgG-Zym phagocytosis in transgenic PLB-985 neutrophils. (A) Time-lapse confocal microscopy was used to monitor IgG-Zym phagocytosis by PLB-985 neutrophils expressing YFP, p67^{phox}-YFP, YFP-p40PX, or YFP-p47PRR. Similarly, phagocytosis was filmed in X-CGD PLB-985 neutrophils stably expressing p67^{phox}-YFP, YFP-p47PRR, or YFP-p40PX as well as PLB-985 cells stably expressing YFP-p47PRR-P366A or YFP-p47PRR-K383E/K385E, as indicated. Arrows indicate the cup of phagosomes (newly forming phagosomes), asterisks indicate the internalized phagosomes. For YFP-p40PX, the upper phagosome was another internalized phagosome appearing at 120 s. Supplementary Movies are available as Supplementary Data. The frames are labeled in seconds with respect to the time at which closure (sealing) of the phagosome was observed, with time zero being the time of closure. Bar, 5 μm. (B) The relative fluorescence intensity on the phagosomal membrane compared with the cytosol was determined in the indicated cell lines for five phagosomes at indicated stages and is shown in the graph as mean ± SE "Internalized" means ≥150 s after phagosome closure. (C) The time for the first appearance of YFP proteins on phagosome membrane of p67^{phox}-YFP, YFP-p40PX, and YFP-p47PRR was analyzed in total of in 18 positive phagosomes for each fluorescently tagged protein, using films from at least four independent experiments for each cell line. The time at which the phagosome is sealed is defined as time zero. The mean ± SD of the times at which membrane translocation was first observed shown, which were significantly different for p67^{phox}, p40PX, and p47PRR (*$p < 0.01$, unpaired t test).

p67^{phox}-YFP, YFP-p47PRR, or, as another control, YFP-p40PX. The level of expression of each YFP-tagged protein in X-CGD PLB-985 lines was similar to that seen in the wild-type PLB-985-derived lines (data not shown). Neither YFP-tagged p67^{phox}, as expected, nor YFP-p47PRR accumulated on IgG-Zym phagosomes in X-CGD PLB-985 cells (Figure 3A; Supplementary Figure S2 and Supplementary Movies S5 and S6). In contrast, YFP-p40PX accumulated on phagosome membranes in X-CGD PLB-985 cells (Figure 3A; Supplementary Movie S7), indicating that the presence of PI(3)P on phagosomes is independent of the presence of flavocytochrome b_{558} and NADPH oxidase activity. We next examined whether YFP-p47PRR derivatives with mutations in the PRR and/or extra-PRR region were able to accumulate on IgG-Zym phagosomes in neutrophil-differentiated PLB-985 cell lines. Although the P366A and K383E/K385E YFP-p47PRR mutants had differential ability to bind to full-length p67^{phox} in vitro (Figure 1), both mutants failed to accumulate on IgG-Zym phagosomes (Figure 3, A and B; Supplementary Movies S8 and S9). This result indicates that the core PRR and the extra-PRR region each contribute to the translocation of YFP-p47PRR to phagosomes. Of note, the double K383E/K385E mutation did not have significant effect on binding to *p67^{phox}* in vitro, but this mutant failed to translocate to phagosomes. Thus, the in vivo system appears to be more sensitive than in vitro assays where proteins are relatively overexpressed. The additional p47PRR mutants shown in Figure 1 also failed to accumulate on phagosomal membranes (not shown), as expected from the in vitro binding data (Figure 1, B and D). Taken together, the above studies provide strong support that recruitment of YFP-p47PRR to the phagosome is mediated by the SH3b domain of p67^{phox}.

IgG-Zym Phagosomes in PLB-985 Neutrophils Are Heterogeneous

In the analysis of images collected by videomicroscopy, it was apparent that not all phagosomes accumulated the p67^{phox}-YFP, YFP-p47PRR, or YFP-p40PX probes and that their presence or absence could be observed even for two phagosomes within the same cell. When analyzing individual phagosomes followed from the time of cup formation for at least 240 s after phagosomal closure, accumulation of the YFP-tagged probe was visible in only 8 of 15 (53%), 6 of 11 (55%), and 6 of 10 (60%) phagosomes in p67^{phox}-YFP–, YFP-p47PRR–, and YFP-p40PX– expressing PLB-985 neutrophils, respectively. Similar results were obtained for the population of phagosomes present 20 min after initiation of the phagocytosis assay, where 100 internalized phagosomes were analyzed in ≥20 fields for each cell line from at least three independent experiments. Only 52 or 53% of internalized phagosomes exhibited accumulation of p67^{phox}-YFP or YFP-p47PRR, respectively, whereas the PI(3)P probe YFP-p40PX was present on 65% of phagosomes. To examine whether translocation of endogenous NADPH oxidase subunits was also heterogeneous, we performed immunolabeling of endogenous p47^{phox}, because we were unable to identify an anti-p67^{phox} antibody suitable for immunostaining.

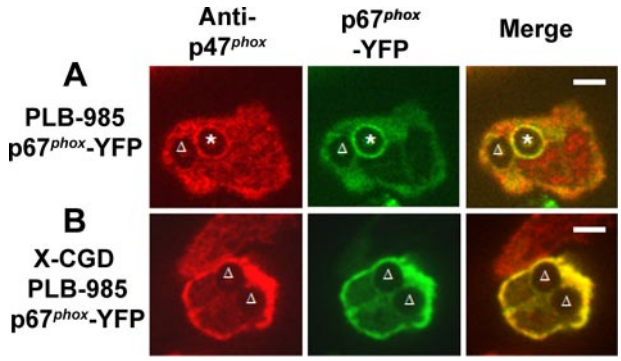

Figure 4. Translocation of endogenous p47^{phox} and p67^{phox}-YFP during phagocytosis of IgG-Zym in PLB-985 cells stably expressing p67^{phox}-YFP. Localization of endogenous p47^{phox} and p67^{phox}-YFP after immunofluorescent staining with anti-p47^{phox} and Alexa555-goat anti-mouse IgG 1 in p67^{phox}-YFP–expressing PLB-985 cells (A), where the asterisk denotes a phagosome with accumulation of both p47^{phox} and p67^{phox}-YFP, or X-CGD PLB-985 cells (B). The triangle indicates negative phagosomes on NADPH oxidase assembly. Representative images from three independent experiments. Bar, 5 μm.

Indirect immunofluorescence of PLB-985 granulocytes expressing p67^{phox}-YFP showed that p47^{phox} accumulated on some IgG-Zym phagosomes but not others (Figure 4A). As expected, p47^{phox} and p67^{phox}-YFP did not accumulate on phagosomes in X-CGD PLB-985 granulocytes (Figure 4B), confirming that p47^{phox} and p67^{phox} membrane translocation is flavocytochrome b_{558}-dependent. Importantly, endogenous p47^{phox} always colocalized with p67^{phox}-YFP, consistent with the translocation of p47^{phox} and p67^{phox} as a unit (Lapouge *et al.*, 2002; Groemping and Rittinger, 2005), and showing that the heterogeneity observed in p67^{phox}-YFP accumulation on phagosomes reflects a heterogeneity in accumulation of endogenous NADPH oxidase subunits. NADPH oxidase activity in IgG-Zym phagosomes, detected using NBT staining combined with videomicroscopy, was consistent with this heterogeneity, showing that ≈50% of phagosomes were oxidase-positive (Supplementary Figure S3).

These observations suggest that IgG-Zym phagosomes in PLB-985 neutrophils are not uniform in their ability to assemble an active oxidase complex or to accumulate PI(3)P. Heterogeneity among phagosomes has been previously recognized and is speculated to reflect variations in the output of signaling networks on individual phagosomes (Griffiths, 2004; Henry *et al.*, 2004). We took advantage of this heterogeneity to design a series of experiments, described below, to investigate the colocalization of p47PRR with p67^{phox}, p40^{phox}, or PI(3)P, using PLB-985 neutrophils coexpressing tagged proteins fluorescing at different wave lengths.

YFP-p47PRR Accumulation on Phagosomes Colocalizes with p67^{phox} and p40^{phox} But Does Not Require p40^{phox} Expression and Is Independent of PI(3)P

The p67^{phox} subunit interacts with p40^{phox} via a high-affinity PB1 motif interaction (Figure 1A). Thus, we anticipated that both p67^{phox} and p40^{phox} might be detected on phagosomes that accumulate p47PRR. First, to simultaneously compare the distribution of p47PRR with that of full-length p67^{phox} or p40^{phox}, we coexpressed mCherry-tagged p47PRR in PLB-985 cells with either p67^{phox}-YFP or YFP-p40^{phox}. mCherry-p47PRR expression was comparable in both cell lines and had no effect on NADPH oxidase activity (data not shown). The accumulation of mCherry-tagged p47PRR on IgG-Zym phagosomes always colocalized with that of coexpressed YFP-tagged p67^{phox} or p40^{phox}, as evident by the simultaneous presence of green and red fluorescence, with a yellow signal when merged (Figure 5A). For example, we analyzed 104 phagosomes in 50 PLB-985 cells coexpressing p67^{phox}-YFP and mCherry-p47PRR, finding that both probes always colocalized, and 53.8% of phagosomes were double positive, similar to the fraction of positive phagosomes observed in PLB-985 cells expressing either p67^{phox}-YFP (53%) or YFP-p47PRR (55%). Overall, these results are consistent with a

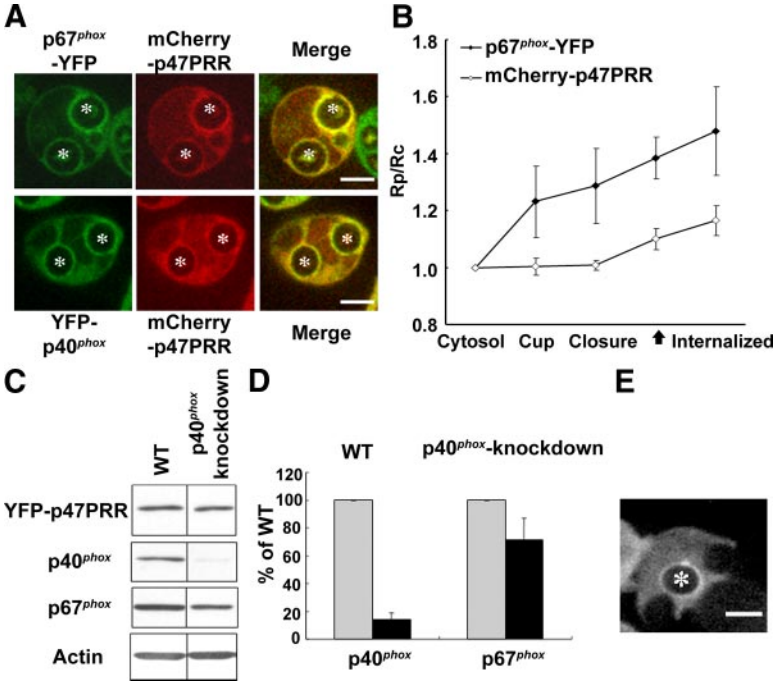

Figure 5. Translocation of YFP-p47PRR during IgG-Zym phagocytosis in p40^{phox} knockdown PLB-985 cells. (A) Colocalization of p67^{phox}-YFP and YFP-p40^{phox} with mCherry-p47PRR on internalized IgG-Zym phagosomes in PLB-985 neutrophils. The green and red fluorescence represent p67^{phox} or p40^{phox}, and p47PRR, respectively. (B) The relative fluorescence intensity on the phagosomal membrane compared with the cytosol was determined in the PLB-985 cells coexpressing p67^{phox} and mCherry-p47PRR for 10 phagosomes at indicated stages and is shown in the graph as mean ± SE. "Internalized" means 222 ± 95 s after phagosome closure (n = 10). The closed arrow on the X-axis indicates the appearance of mCherry-p47PRR on phagosome. (C) Expression of YFP-p47PRR, p40^{phox}, p67^{phox}, and actin was determined by immunoblotting. (D) Densitometry analysis of p40^{phox} and p67^{phox} expression normalized to actin from three independent experiments. (E) Localization of YFP-p47PRR in p40^{phox} knockdown PLB-985 cells during IgG-Zym phagocytosis. Bar, 5 μm.

model in which $p67^{phox}$ on internalized phagosomal membranes is bound to both the 47PRR probe and to $p40^{phox}$.

Simultaneous imaging of probe accumulation on individual phagosomes in cells coexpressing $p67^{phox}$-YFP and mCherry-p47PRR showed that $p67^{phox}$-YFP accumulated on the phagosome cup ≈30 s before closure, before the appearance of the PRR probe, and was retained after internalization (Figure 5B; Supplementary Movie S10), similar to PLB-985 neutrophils expressing $p67^{phox}$-YFP alone (Figure 3B). mCherry-p47PRR appeared ≈60 s after phagosome closure (Figure 5B; Supplementary Movie S10), similar to YFP-p47PRR (Figure 3B). The relative intensity of the mCherry-p47PRR fluorescent signal on phagosomes is somewhat lower than that observed in YFP-p47PRR, probably related to differences due to the different fluorescent tags.

The $p40^{phox}$ subunit contains an SH3 domain that is a second potential target of p47PRR, although the affinity of p47PRR for the $p40^{phox}$ SH3 domain is ≈250-fold lower than for the $p67^{phox}$ SH3b domain (Ito *et al.*, 1996; Grizot *et al.*, 2001; Lapouge *et al.*, 2002; Massenet *et al.*, 2005). To exclude that p47PRR membrane recruitment involves the SH3 domain of $p40^{phox}$, we expressed YFP-p47PRR in $p40^{phox}$-knockdown PLB-985 cells. Western blotting showed that YFP-p47PRR expression in the $p40^{phox}$ knockdown cells was similar to the wild-type PLB-985 line expressing transgenic p47PRR, whereas $p40^{phox}$ expression was decreased by 86 ± 5% (n = 3; Figure 5, C and D). We also observed a modest decrease of 29 ± 16% in $p67^{phox}$ expression (Figure 5, C and D) in $p40^{phox}$-deficient cells, similar to the reduced $p67^{phox}$ levels reported in neutrophils from $p40^{phox}$ knockout mice (Ellson *et al.*, 2006b). Despite the marked decrease in $p40^{phox}$ expression in $p40^{phox}$ knockdown PLB-985 cells (Figure 4D), videomicroscopy showed that YFP-p47PRR accumulated on phagosome membranes after internalization (Figure 5E) with a time course similar to the kinetics in PLB-985 cells with normal expression of $p40^{phox}$ (Figure 3, B and C). Examination of internalized phagosomes in $p40^{phox}$ knockdown cells after 20 min of phagocytosis showed that 52% (128/244) were YFP-p47PRR-positive, similar to the frequency observed in PLB-985 expressing YFP-p47PRR (see above). Thus, the colocalization of p47PRR with $p67^{phox}$ on internalized phagosomes (Figure 5A) and the detection of p47PRR translocation in $p40^{phox}$ knockdown cells (Figure 5E) provide further support that this probe targets the SH3b domain of $p67^{phox}$.

YFP-p47PRR Accumulation on Phagosomes Is Independent of PI(3)P and NADPH Oxidase Activity

The recruitment of the p40PX domain probe for PI(3)P precedes the accumulation of p47PRR on internalized phagosomes by ≈30 s (Figure 3C). This temporal relationship suggested that PI(3)P might be involved in the loss of the tail-to-tail interaction between $p47^{phox}$ and $p67^{phox}$. To investigate this, we coexpressed mCherry-tagged p40PX in PLB-985 cells with either $p67^{phox}$-YFP or YFP-p47PRR in order to simultaneously examine their recruitment on individual phagosome and also examined the effect of the PI3K inhibitor wortmannin.

In PLB-985 cells coexpressing $p67^{phox}$-YFP and mCherry-p40PX, we observed colocalization of both probes on many phagosomes, with the former first accumulating in the phagosomal cup and the mCherry-p40PX probe appearing after internalization (≈30 s; Figure 6A, phagosome b and c, and C; Supplementary Movie S11), similar to the time course shown in Figure 3C. However, some phagosomes only had $p67^{phox}$-YFP accumulation without mCherry-p40PX translocation (Figure 6A, phagosome a; Supplementary Figure S4A, phagosome g), other phagosomes accumulated only mCherry-p40PX (Supplementary Figure S4A, phagosome f), and some phagosomes showed no accumulation of either probe (Supplementary Figure S4A, phagosome e). Similar results were seen for cells coexpressing mCherry-p40PX and YFP-p47PRR. These probes accumulated sequentially on IgG-Zym phagosomes at ≈30 and ≈60 s, respectively, after phagosome closure (Figure 6, B, phagosome d, and D; Supplementary Movie S12), consistent with kinetic studies in cells expressing a single fluorescent protein (Figure 3C). However, some phagosomes had neither mCherry-p40PX nor YFP-p47PRR (Supplementary Figure S4B, phagosome l), even in cells where other phagosomes showed accumulation of both probes (Supplementary Figure S4B, phagosomes h and i). In other phagosomes, membrane translocation of mCherry-p40PX and YFP-p47PRR occurred independently of each other (Supplementary Figure S4B, phagosomes j and k). Thus, for phagosomes that accumulated either of the NADPH oxidase probes, $p67^{phox}$-YFP and YFP-p47PRR, along with the PI(3)P probe, recruitment followed a reproducible sequence. However, other phagosomes accumulated either the NADPH oxidase probe or the PI(3)P probe.

We also evaluated the presence or absence of fluorescent proteins on the population of IgG-Zym phagosomes present after 20 min after initiation of the phagocytosis assay. Three hundred individual phagosomes from at least three independent experiments were analyzed. In PLB-985 neutrophils coexpressing $p67^{phox}$-YFP and mCherry-p40PX, 42.3% phagosomes were positive for both probes. There were 11.7% of phagosomes that were only $p67^{phox}$-YFP–positive, 22.0% only positive for mCherry-p40PX, and 24.0% that did not accumulate either probe. Similar results were observed in PLB-985 cells expressing YFP-p47PRR and mCherry-p40PX. This analysis supports the imaging studies of individual phagosomes (Figure 6, A and B; Supplementary Figure S4), showing that the $p67^{phox}$-YFP and the p47PRR probes accumulate on phagosomes independent of the p40PX probe. We also observed that phagosome translocation of both $p67^{phox}$ and p47PRR was wortmannin-resistant, whereas, as expected, p40PX phagosome membrane accumulation was wortmannin-sensitive (Figure 7, A and B). Taken together with the videomicroscopy analysis (Figure 6), these results show that PI(3)P accumulation does not always correlate with assembly of $p67^{phox}$ or its p47PRR probe on the phagosome, and thus PI(3)P does not appear to regulate access to the p67SH3b domain.

Because phagosome NADPH oxidase activity is markedly inhibited by wortmannin (Ellson *et al.*, 2006a,b; Suh *et al.*, 2006; Tian *et al.*, 2008), the failure of wortmannin to prevent phagosomal accumulation of the p47PRR probe suggests that this event is also independent of NADPH oxidase activity. To further test this, we pretreated PLB-985 granulocytes expressing $p67^{phox}$-YFP or YFP-p47PRR with the NADPH oxidase flavocytochrome inhibitor DPI (O'Donnell *et al.*, 1993; Cross *et al.*, 1994) before stimulation with IgG-Zym. As expected, superoxide production in phagosomes was profoundly inhibited when PLB-985 granulocytes were pretreated with DPI (Figure 7C). However, the phagosomal translocation of both $p67^{phox}$-YFP and YFP-p47PRR in DPI-pretreated cells (Figure 7D, phagosomes p and q) was similar to non-DPI-treated cells (Figure 3), indicating that the dissociation of the $p47^{phox}$/$p67^{phox}$ tail-to-tail is not a consequence of NADPH oxidase activity.

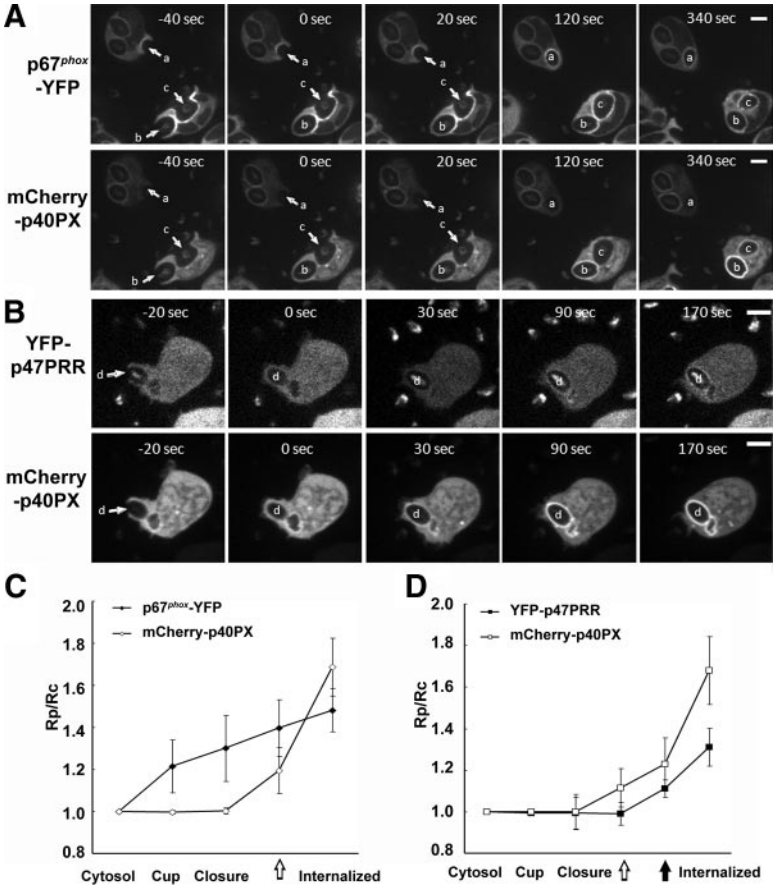

Figure 6. Accumulation of p67^{phox}-YFP and YFP-p47PRR with mCherry-p40PX on the phagosome during IgG-Zym phagocytosis in PLB-985 neutrophils. Time-lapse confocal microscopy was used to monitor translocation of coexpressed or p67^{phox} and mCherry-p40PX (A) YFP-p47PRR and mCherry-p40PX (B) in PLB-985 cells during IgG-Zym phagocytosis. Arrows indicate the cup of phagosomes (newly forming phagosomes), and letters a–d indicate individual internalized phagosomes. The frames are labeled in seconds with respect to the time at which closure (sealing) of the phagosome was observed, with time zero being the time of closure. Bar, 5 μm. Supplementary Movies S11 and S12 are available as Supplementary Data. The relative fluorescence intensity on the phagosomal membrane compared with the cytosol was determined in the PLB-985 cells coexpressing p67^{phox}-YFP and mCherry-p40PX (C) or YFP-p47PRR and mCherry-p40PX (D). Five phagosomes for each cell line were analyzed at the indicated stages, which are shown in the graph as mean ± SE. "Internalized" means 146 ± 82 and 170 ± 62 s for C and D, respectively, after phagosome closure. The open and closed arrows indicate the appearance of mCherry-p40PX and YFP-p47PRR, respectively, on the phagosome.

Access of p47PRR to the SH3b Domain of p67^{phox} Does Not Correlate with Termination of Oxidase Activity

The accessibility of SH3b domain of p67^{phox} to the p47PRR probe after phagosome sealing is consistent with the dissociation of the tail-to-tail interaction between p47^{phox} and p67^{phox}. We examined whether this correlates with cessation of NADPH oxidase activity. To monitor the time course of oxidant production within individual phagosomes, PLB-985 granulocytes were stimulated with BSA immune complexes covalently labeled with dichlorodihydrofluorescein (H_2DCF; Fc OxyBURST Green), which are taken up by FcγR receptors (Ryan *et al.,* 1990). NADPH oxidase activation results in the oxidation of nonfluorescent H_2DCF to green fluorescent DCF (Ryan *et al.,* 1990). To facilitate visualization of cells during fluorescence videomicroscopy, we used PLB-985 cells expressing mCherry-tagged p40PX, which gives a brighter signal on phagosomes than mCherry-p47PRR (Figures 5B and 6D). Phagocytosis of Fc OxyBURST particles was recorded with 568- and 488-nm excitation to monitor fluorescence of each probe, respectively. mCherry-p40PX accumulated on Fc OxyBURST phagosomes after internalization, as expected (Figure 8A). A faint green fluorescent

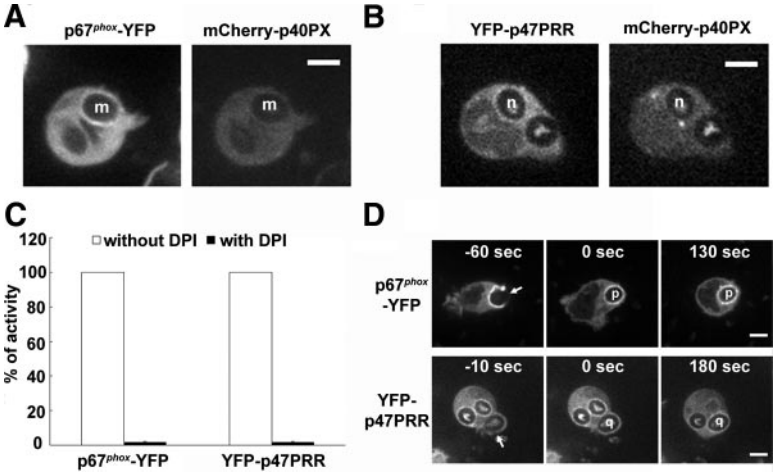

Figure 7. Accumulation of NADPH oxidase probes on the phagosome during IgG-Zym phagocytosis in PLB-985 neutrophils treated with wortmannin or DPI. Translocation of p67^{phox}-YFP (A) and YFP-p47PRR (B) during IgG-Zym phagocytosis in transgenic PLB-985 neutrophils coexpressing mCherry-p40PX in the presence of 100 nM wortmannin. Letters m and n indicate individual internalized phagosomes. PLB-985 granulocytes expressing p67^{phox}-YFP or YFP-p47PRR were pretreated with 10 μM DPI at 37°C for 15 min, followed with synchronized phagocytosis as described in *Materials and Methods.* NADPH oxidase activity was measured in the presence of luminal, SOD, and catalase. Results are expressed as total relative light unit (RLU) values more than 45 min, measured at 1-min intervals. (C) Values represent the mean ± SD of triplicate determinations. Live image was monitored using confocal microscopy as described in Figure 3A. (D) Arrows indicate presealing (newly forming phagosomes) and letters o and p indicates internalized phagosome. Time-lapse confocal microscopy was used as described in Figure 3A. Bar, 5 μm.

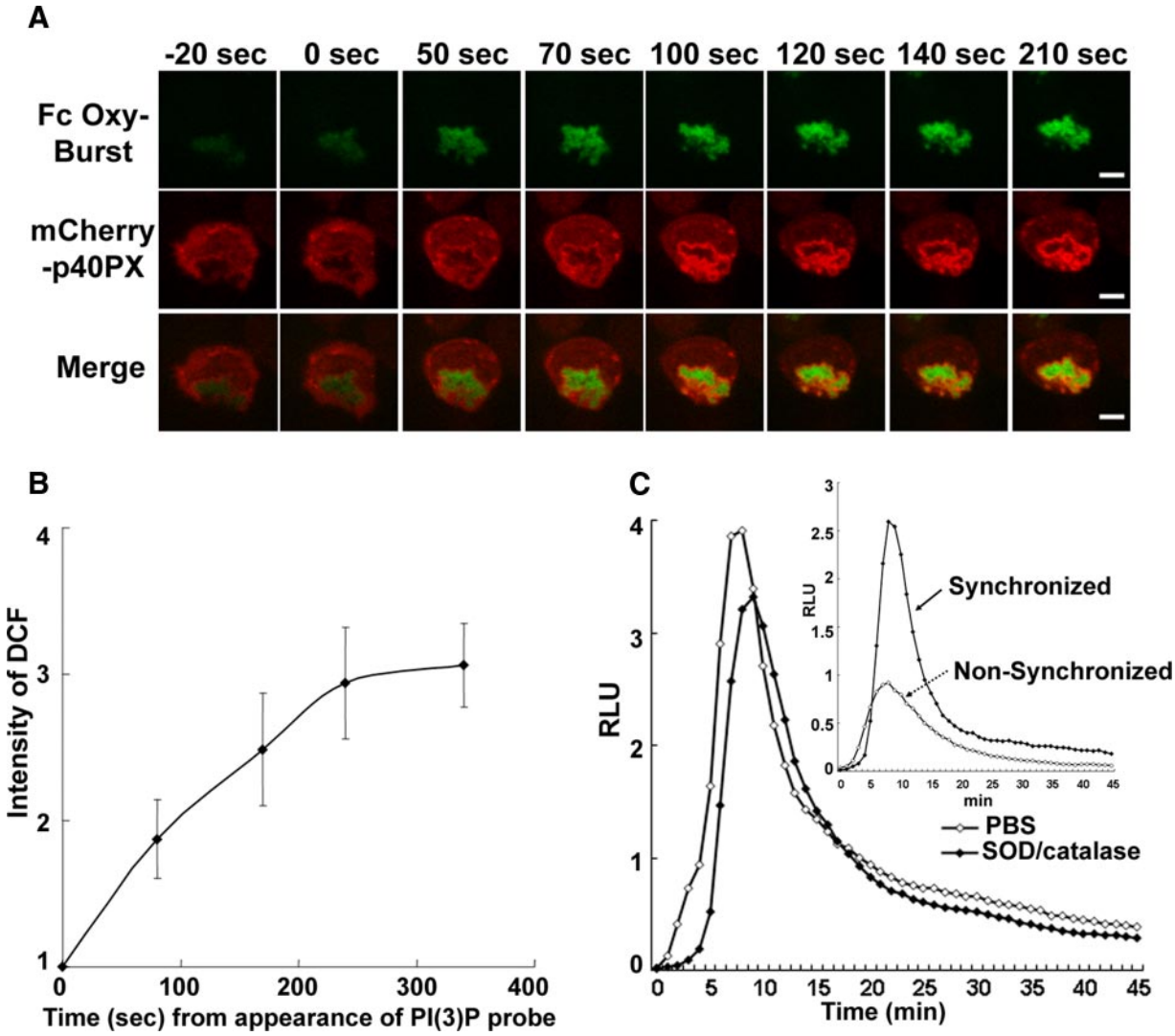

Figure 8. Activation of the NADPH oxidase in Fc OxyBURST phagosomes. (A) Superoxide production was monitored in individual phagosomes after the addition of Fc OxyBURST to PLB-985 neutrophils expressing mCherry-p40PX. The green and red fluorescence represent DCF (a probe for H_2O_2) and mCherry-p40PX, respectively. The frames are labeled in seconds with respect to the time at which closure (sealing) of the phagosome was observed, with time zero being the time of closure. (B) The relative intensity of DCF fluorescence in five phagosomes from three independent experiments was analyzed with Image J software. The intensity of DCF was considered as 1.0 at the time at which mCherry-p40PX first appeared on internalized phagosomes and is shown over time (s) after the appearance of the mCherry-p40PX probe. (C) Phagosome superoxide production induced by Fc OxyBURST was measured for 46 min by chemiluminescence in the presence of 20 μM luminol, with or without SOD and catalase. The inset shows the intracellular phagosome superoxide production measured for 46 min in PLB-985 cells expressing mCherry-p40PX, using nonsynchronized (as described in Figure 2D) or synchronized phagocytosis method, as indicated.

signal was detected upon initial binding of Fc OxyBURST to cells, indicating that superoxide production begins before sealing. Fc OxyBURST fluorescence became progressively brighter after phagosomal closure and increased over at least the next 5 min (Figure 8, A and B), indicating that superoxide production continues for many minutes after the time at which YFP-p47PRR first appears on IgG-Zym phagosomes (61 ± 20 s after closure, Figure 3C). This result indicates that the tail-to-tail dissociation of $p47^{phox}/p67^{phox}$ does not correlate with cessation of NADPH oxidase activity within phagosomes.

To confirm that oxidant production increases within Fc OxyBURST phagosomes and is sustained after their internalization, we monitored the kinetics of Fc OxyBURST-stimulated NADPH oxidase activity in mCherry-p40PX PLB-985 neutrophils using luminol-enhanced chemiluminescence to detect oxidant production (Dahlgren and Karlsson, 1999). To synchronously activate the cells, Fc OxyBURST was bound to PLB-985 neutrophils at 4°C, and cells then activated by the addition of prewarmed media containing luminol. This luminol-enhanced chemiluminescence was largely resistant to SOD and catalase (Figure 8C), consistent with detection of oxidants produced within phagosomes, and rapidly increased after 3–4 min to peak at ≈10 min, followed by a gradual decline (Figure 8C). No signal was detected from X-CGD PLB-985 cells (not shown), verifying that Fc OxyBURST-induced chemiluminescence reflects NADPH oxidase activity. Note that because cells were initially at 4°C for synchronization of phagocytosis, the increase in Fc OxyBURST-stimulated oxidant production in the first few minutes was somewhat delayed compared with cells maintained at 37°C as in the imaging studies (Figure 8A) or in a nonsynchronized chemiluminescence assay (Figure 8C, inset).

DISCUSSION

In this study, we examined phagocytosis-induced NADPH oxidase assembly and explored the dynamics of a tail-to-tail interaction between the NADPH oxidase subunits p47^{phox} and p67^{phox} that is crucial for recruitment of p67^{phox} in neutrophils to activate flavocytochrome b_{558}. The C-terminal SH3b domain of p67^{phox} binds to the proline-rich C-terminus of the p47^{phox}, which contains both a core PxxP motif and an adjacent "extra-PRR" region that each contribute to a high-affinity interaction between these two subunits (Finan *et al.*, 1994; Leto *et al.*, 1994; Leusen *et al.*, 1995; de Mendez *et al.*, 1996; Morozov *et al.*, 1998; Kami *et al.*, 2002; Lapouge *et al.*, 2002; Massenet *et al.*, 2005; Mizuki *et al.*, 2005). Using confocal videomicroscopy of PLB-985 neutrophils ingesting IgG-opsonized zymosan particles, we showed that a YFP-tagged protein corresponding to the C-terminus of p47^{phox}, YFP-p47PRR, appeared on phagosomes ≈60 s after sealing and internalization. This lagged the appearance of p67^{phox}-YFP, which first accumulated on the cup of newly formed phagosome as previously shown (Allen *et al.*, 1999; van Bruggen *et al.*, 2004) and of PI(3)P, which was detected shortly after internalization. The delayed translocation of YFP-p47PRR is consistent with a scenario in which the SH3b domain of p67^{phox} is masked by an intermolecular interaction with the tail of p47^{phox} during the initial phases of oxidase assembly on the phagosome, but becomes accessible after phagosome internalization and recruits the YFP-p47PRR probe. Interestingly, the p67^{phox}/p47^{phox} tail-to-tail interaction may be acquired as an early priming event before translocation of the cytosolic *phox* complex to the NADPH oxidase flavocytochrome *b* (Brown *et al.*, 2003). The current study suggests that this tail-to-tail interaction is dispensed with after the assembly of the NADPH oxidase on phagosomes.

That the SH3b domain of p67^{phox} is the target of the p47PRR probe is supported by a variety of findings. The interaction between these two domains is mediated both by the core PxxP sequence in p47^{phox} and by amino acids just downstream of this PxxP motif, which leads to high affinity and specificity for the p67^{phox} SH3b domain (Kami *et al.*, 2002; Lapouge *et al.*, 2002; Li, 2005; Massenet *et al.*, 2005; Mizuki *et al.*, 2005). Importantly, we saw no translocation for p47PRR derivatives harboring mutations in either the core PxxP motif or the adjacent extra-PRR region, providing very strong support that this probe targets p67^{phox}. Additional evidence supporting the specificity of the p47PRR probe for p67^{phox} includes faithful colocalization of p67^{phox} and the p47PRR on phagosomes in experiments using different fluorescent labels to tag each protein and the dependence of both p67^{phox} and p47PRR on flavocytochrome *b* for membrane translocation. Finally, an alternative potential target for YFP-p47PRR is the SH3 domain of p40^{phox}, which also exhibits binding to the C-terminal PRR region of p47^{phox}, albeit with ≈250-fold less affinity than for the SH3b domain of p67^{phox} (Massenet *et al.*, 2005). However, the p47PRR probe still accumulated on phagosomes in p40^{phox} knockdown cells, consistent with the assignment of p67^{phox} SH3b as the target of p47PRR.

The events that regulate the dissociation of the tail-to-tail interaction between p47^{phox} and p67^{phox}, leading to accessibility of the p67^{phox} SH3 domain to the p47PRR probe, remain to be clarified. The accumulation of the p47PRR probe temporally followed the appearance of PI(3)P on internalized phagosomes, which binds to the p40^{phox} subunit to stimulate phagosomal enzyme activity (Ellson *et al.*, 2006a,b; Suh *et al.*, 2006; Tian *et al.*, 2008). However, PI(3)P or other PI3K-dependent events do not appear to regulate access to the p67^{phox} SH3b domain, because YFP-p47PRR was detected on phagosomes that lacked PI(3)P, and membrane translocation of both YFP-tagged p67^{phox} and p47PRR was insensitive to the PI3K inhibitor, wortmannin. Because wortmannin inhibits phagosomal NADPH oxidase activity (Suh *et al.*, 2004; Ellson *et al.*, 2006a,b; Tian *et al.*, 2008), this result also suggests that exposure of the p67^{phox} SH3b domain is independent of NADPH oxidase activity, which was verified in studies using DPI to inhibit electron transfer through the flavocytochrome *b*. Both p47^{phox} and p67^{phox} are phosphorylated after cellular activation, which could potentially lead to loss of their tail-to-tail interaction. Multiple serine/threonine kinases have been implicated in phosphorylation of the p47^{phox} subunit, which begins in the cytosol and increases after p47^{phox} translocation to the membrane (Vignais, 2002; Nauseef, 2004; Groemping and Rittinger, 2005). However, the order in which each of the 11 serines identified as phosphorylation sites are modified and the functional consequence are incompletely understood, with the exception of Ser 303, 304, and 328, whose phosphorylation enables the unmasking of adjacent tandem SH3 domains that target p47^{phox} to p22^{phox}. Of note, the PRR/extra-PRR region in the C-terminus of p47^{phox} is flanked by potential serine phosphorylation sites at residues 359, 370, and 379. Recent in vitro studies indicate that phosphorylation of Ser379 but not Ser359/370 destabilizes the otherwise high-affinity interaction between the p67^{phox} SH3b domain and C-terminal region of p47^{phox} (Massenet *et al.*, 2005). Thus, it is attractive to speculate that phosphorylation of p47^{phox} Ser379 occurs after phagosomal closure and results in the dissociation of the tail-to-tail interaction with p67^{phox}. However, it is difficult to test this hypothesis experimentally, because initial membrane translocation of p67^{phox} is dependent on its tail-to-tail interaction with p47^{phox}, and substitution of p47^{phox} Ser379 with either an alanine or aspartate prevents the recruitment of p67^{phox} to the membrane (Faust *et al.*, 1995; Mizuki *et al.*, 2005).

A second remaining question is the functional significance of the change in the tail-to-tail interaction between p47^{phox} and p67^{phox} after phagosome internalization. Real-time imaging of NADPH oxidase activity using Fc OxyBURST Green showed that oxidant production continued in internalized phagosomes beyond the time at which the YFP-p47PRR probe is recruited, indicating that the dissociation of p47^{phox}/p67^{phox} tail-to-tail interaction is not a marker for phagosomes that cease to generate superoxide. That superoxide production continues after loss of the tail-to-tail interaction is consistent with studies showing that truncated forms of p67^{phox} lacking the C-terminus can support NADPH oxidase activity in model systems (de Mendez *et al.*, 1994, 1996; Leusen *et al.*, 1995; Hata *et al.*, 1998; Arias *et al.*, 2004). It is possible that modification of the network of interactions that contribute to formation of the NADPH oxidase complex is important for sustained activity after assembly. For example, the C-terminus of p47^{phox} may be retargeted to the SH3 domain of p40^{phox}. Indeed, mutations in the p40^{phox} SH3 domain reduce NADPH oxidase activity (Suh *et al.*, 2006; Bissonnette *et al.*, 2008; Tian *et al.*, 2008). Finally, photobleaching studies of fluorescently tagged p67^{phox} suggest that p67^{phox} is continuously cycling on and off phagosome membranes, and thus loss of the tail-to-tail association with p47^{phox} may be necessary for p67^{phox} to be shed from the phagosome.

In conclusion, this study defines a sequence of events during phagocytosis-induced NADPH oxidase assembly and provides experimental evidence that protein–protein

interactions within the NADPH oxidase complex are dynamic and are modulated after its assembly on the phagosome. A YFP-tagged C-terminus of $p47^{phox}$ is a promising probe for monitoring status of the tail-to-tail interaction between $p47^{phox}$ and $p67^{phox}$. The SH3b domain of $p67^{phox}$ becomes accessible to this probe after phagosome internalization after, although not dependent on, the accumulation of PI(3)P on the phagosome membrane. The molecular mechanism of the $p47^{phox}/p67^{phox}$ tail-to-tail dissociation is under investigation in our laboratory, which may help us to better understand the inter- and intramolecular rearrangements of oxidase complex that regulate NADPH oxidase activity during phagocytosis.

ACKNOWLEDGMENTS

We thank Joel Swanson, Lynn Kamen, and members of the Dinauer lab for helpful discussions and Shari Upchurch for assistance with manuscript preparation. We thank the Indiana Center for Biological Microscopy, which was supported in part by a grant (INGEN) from Lilly Endowment. This work was supported by National Institutes of Health Grants R01 HL45635 (M.C.D. and S.A.), the Canadian Institutes for Health Research (S.G.), the Riley Children's Foundation (M.C.D.), and the Indiana University Simon Cancer Center (P30 CA082709) Flow Cytometry Core and Indiana Center for Biological Microscopy (the latter is also supported in part by a grant from Lilly Endowment).

REFERENCES

Allen, L. A., DeLeo, F. R., Gallois, A., Toyoshima, S., Suzuki, K., and Nauseef, W. M. (1999). Transient association of the nicotinamide adenine dinucleotide phosphate oxidase subunits p47phox and p67phox with phagosomes in neutrophils from patients with X-linked chronic granulomatous disease. Blood *93*, 3521–3530.

Arias, A. A., Matute, J. D., Patino, P., and Dinauer, M. (2004). Analysis of a p67phox Δ401 mutant identified in chronic granulomatous disease: deletion of C-terminal SH3 binding site for p47phox still supports NADPH oxidase activity in COSphox cells. Blood *104*, 654a.

Bissonnette, S. A., Glazier, C. M., Stewart, M. Q., Brown, G. E., Ellson, C. D., and Yaffe, M. B. (2008). Phosphatidylinositol 3-phosphate-dependent and -independent functions of p40phox in activation of the neutrophil NADPH oxidase. J. Biol. Chem. *283*, 2108–2119.

Brown, G. E., Stewart, M. Q., Liu, H., Ha, V. L., and Yaffe, M. B. (2003). A novel assay system implicates PtdIns(3,4)P(2), PtdIns(3)P, and PKC delta in intracellular production of reactive oxygen species by the NADPH oxidase. Mol. Cell *11*, 35–47.

Cross, A., Yarchover, J., and Curnutte, J. (1994). A novel diaphorase activity associated with the superoxide-generating NADPH-oxidase of human neutrophils. J. Biol. Chem. *269*, 21448–21454.

Dahlgren, C., and Karlsson, A. (1999). Respiratory burst in human neutrophils. J. Immunol. Methods *232*, 3–14.

de Mendez, I., Adams, A., Sokolic, R., Malech, H., and Leto, T. (1996). Multiple SH3 domain interactions regulate NADPH oxidase assembly in whole cells. EMBO J. *15*, 1211–1220.

de Mendez, I., Garrett, M. C., Adams, A. G., and Leto, T. L. (1994). Role of p67-phox SH3 domains in assembly of the NADPH oxidase system. J. Biol. Chem. *269*, 16326–16332.

DeLeo, F. R., Allen, L. A., Apicella, M., and Nauseef, W. M. (1999). NADPH oxidase activation and assembly during phagocytosis. J. Immunol. *163*, 6732–6740.

Dinauer, M. (2003). The phagocyte system and disorders of granulopoiesis and granulocyte function. In: Nathan and Oski's Hematology of Infancy and Childhood, Vol. 1, ed. D. G. Nathan, S. H. Orkin, D. Ginsburg, and A. T. Look, Philadelphia: WB Saunders, 923–1010.

Dusi, S., Della Bianca, V., Donini, M., Nadalini, K. A., and Rossi, F. (1996). Mechanisms of stimulation of the respiratory burst by TNF in nonadherent neutrophils: its independence of lipidic transmembrane signaling and dependence on protein tyrosine phosphorylation and cytoskeleton. J. Immunol. *157*, 4615–4623.

el Benna, J., Faust, L. P., and Babior, B. M. (1994). The phosphorylation of the respiratory burst oxidase component p47phox during neutrophil activation. Phosphorylation of sites recognized by protein kinase C and by proline-directed kinases. J. Biol. Chem. *269*, 23431–23436.

Ellson, C., Davidson, K., Anderson, K., Stephens, L. R., and Hawkins, P. T. (2006a). PtdIns3P binding to the PX domain of p40phox is a physiological signal in NADPH oxidase activation. EMBO J. *25*, 4468–4478.

Ellson, C. D., Anderson, K. E., Morgan, G., Chilvers, E. R., Lipp, P., Stephens, L. R., and Hawkins, P. T. (2001). Phosphatidylinositol 3-phosphate is generated in phagosomal membranes. Curr. Biol. *11*, 1631–1635.

Ellson, C. D., Davidson, K., Ferguson, G. J., O'Connor, R., Stephens, L. R., and Hawkins, P. T. (2006b). Neutrophils from p40phox-/- mice exhibit severe defects in NADPH oxidase regulation and oxidant-dependent bacterial killing. J. Exp. Med. *203*, 1927–1937.

Faust, L. R., el Benna, J., Babior, B. M., and Chanock, S. J. (1995). The phosphorylation targets of p47phox, a subunit of the respiratory burst oxidase. Functions of the individual target serines as evaluated by site-directed mutagenesis. J. Clin. Invest. *96*, 1499–1505.

Finan, P., Shimizu, Y., Gout, I., Hsuan, J., Truong, O., Butcher, C., Bennett, P., Waterfield, M., and Kellie, S. (1994). An SH3 domain and proline-rich sequence mediate an interaction between two components of the phagocyte NADPH oxidase complex. J. Biol. Chem. *269*, 13752–13755.

Fontayne, A., Dang, P. M., Gougerot-Pocidalo, M. A., and El-Benna, J. (2002). Phosphorylation of p47phox sites by PKC alpha, beta II, delta, and zeta: effect on binding to p22phox and on NADPH oxidase activation. Biochemistry *41*, 7743–7750.

Greenberg, S., Burridge, K., and Silverstein, S. C. (1990). Colocalization of F-actin and talin during Fc receptor-mediated phagocytosis in mouse macrophages. J. Exp. Med. *172*, 1853–1856.

Griffiths, G. (2004). On phagosome individuality and membrane signalling networks. Trends Cell Biol. *14*, 343–351.

Grizot, S., *et al.* (2001). Small angle neutron scattering and gel filtration analyses of neutrophil NADPH oxidase cytosolic factors highlight the role of the C-terminal end of p47phox in the association with p40phox. Biochemistry *40*, 3127–3133.

Groemping, Y., Lapouge, K., Smerdon, S. J., and Rittinger, K. (2003). Molecular basis of phosphorylation-induced activation of the NADPH oxidase. Cell *113*, 343–355.

Groemping, Y., and Rittinger, K. (2005). Activation and assembly of the NADPH oxidase: a structural perspective. Biochem. J. *386*, 401–416.

Hata, K., Ito, T., Takeshige, K., and Sumimoto, H. (1998). Anionic amphiphile-independent activation of the phagocyte NADPH oxidase in a cell-free system by p47phox and p67phox, both in C terminally truncated forms. Implication for regulatory Src homology 3 domain-mediated interactions. J. Biol. Chem. *273*, 4232–4236.

Hata, K., Takeshige, K., and Sumimoto, H. (1997). Roles for proline-rich regions of p47phox and p67phox in the phagocyte NADPH oxidase activation in vitro. Biochem. Biophys. Res. Commun. *241*, 226–231.

Henry, R. M., Hoppe, A. D., Joshi, N., and Swanson, J. A. (2004). The uniformity of phagosome maturation in macrophages. J. Cell Biol. *164*, 185–194.

Heyworth, P. G., Curnutte, J. T., Nauseef, W. M., Volpp, B. D., Pearson, D. W., Rosen, H., and Clark, R. A. (1991). Neutrophil nicotinamide adenine dinucleotide phosphate oxidase assembly. Translocation of p47-phox and p67-phox requires interaction between p47-phox and cytochrome b558. J. Clin. Invest. *87*, 352–356.

Ito, T., Matsui, Y., Ago, T., Ota, K., and Sumimoto, H. (2001). Novel modular domain PB1 recognizes PC motif to mediate functional protein-protein interactions. EMBO J. *20*, 3938–3946.

Ito, T., Nakamura, R., Sumimoto, H., Takeshige, K., and Sakaki, Y. (1996). An SH3 domain-mediated interaction between the phagocyte NADPH oxidase factors p40phox and p47phox. FEBS Lett. *385*, 229–232.

Kami, K., Takeya, R., Sumimoto, H., and Kohda, D. (2002). Diverse recognition of non-PxxP peptide ligands by the SH3 domains from p67(phox), Grb2 and Pex13p. EMBO J. *21*, 4268–4276.

Lapouge, K., Smith, S. J., Groemping, Y., and Rittinger, K. (2002). Architecture of the p40–p47-p67phox complex in the resting state of the NADPH oxidase. A central role for p67phox. J. Biol. Chem. *277*, 10121–10128.

Leto, T. L., Adams, A. G., and de Mendez, I. (1994). Assembly of the phagocyte NADPH oxidase: binding of Src homology 3 domains to proline-rich targets. Proc. Natl. Acad. Sci. USA *91*, 10650–10654.

Leusen, J. H., Fluiter, K., Hilarius, P. M., Roos, D., Verhoeven, A. J., and Bolscher, B. G. (1995). Interactions between the cytosolic components p47phox and p67phox of the human neutrophil NADPH oxidase that are not required for activation in the cell-free system. J. Biol. Chem. *270*, 11216–11221.

Li, S., Yamauchi, A., Marchal, C. C., Molitoris, J. K., Quilliam, L. A., and Dinauer, M. C. (2002). Chemoattractant-stimulated Rac activation in wild-

type and Rac2-deficient murine neutrophils: preferential activation of Rac2 and Rac2 gene dosage effect on neutrophil functions. J. Immunol. *169*, 5043–5051.

Li, S. S. (2005). Specificity and versatility of SH3 and other proline-recognition domains: structural basis and implications for cellular signal transduction. Biochem. J. *390*, 641–653.

Li, X. J., Grunwald, D., Mathieu, J., Morel, F., and Stasia, M. J. (2005). Crucial role of two potential cytosolic regions of Nox2, 191TSSTKTIRRS200 and 484DESQANHFAVHHDEEKD500, on NADPH oxidase activation. J. Biol. Chem. *280*, 14962–14973.

Massenet, C., Chenavas, S., Cohen-Addad, C., Dagher, M. C., Brandolin, G., Pebay-Peyroula, E., and Fieschi, F. (2005). Effects of p47phox C terminus phosphorylations on binding interactions with p40phox and p67phox. Structural and functional comparison of p40phox and p67phox SH3 domains. J. Biol. Chem. *280*, 13752–13761.

Ming, W., Li, S., Billadeau, D. D., Quilliam, L. A., and Dinauer, M. C. (2007). The Rac effector p67phox regulates phagocyte NADPH oxidase by stimulating Vav1 guanine nucleotide exchange activity. Mol. Cell. Biol. *27*, 312–323.

Mizuki, K., Takeya, R., Kuribayashi, F., Nobuhisa, I., Kohda, D., Nunoi, H., Takeshige, K., and Sumimoto, H. (2005). A region C-terminal to the proline-rich core of p47phox regulates activation of the phagocyte NADPH oxidase by interacting with the C-terminal SH3 domain of p67phox. Arch. Biochem. Biophys. *444*, 185–194.

Morozov, I., Lotan, O., Joseph, G., Gorzalczany, Y., and Pick, E. (1998). Mapping of functional domains in p47(phox) involved in the activation of NADPH oxidase by "peptide walking." J. Biol. Chem. *273*, 15435–15444.

Nauseef, W. M. (2004). Assembly of the phagocyte NADPH oxidase. Histochem. Cell Biol. *122*, 277–291.

O'Donnell, B. V., Tew, D. G., Jones, O. T., and England, P. J. (1993). Studies on the inhibitory mechanism of iodonium compounds with special reference to neutrophil NADPH oxidase. Biochem. J. *290*(Pt 1), 41–49.

Price, M. O., Atkinson, S. J., Knaus, U. G., and Dinauer, M. C. (2002). Rac activation induces NADPH oxidase activity in transgenic COSphox cells, and the level of superoxide production is exchange factor-dependent. J. Biol. Chem. *277*, 19220–19228.

Ryan, T. C., Weil, G. J., Newburger, P. E., Haugland, R., and Simons, E. R. (1990). Measurement of superoxide release in the phagovacuoles of immune complex-stimulated human neutrophils. J. Immunol. Methods *130*, 223–233.

Shaner, N. C., Campbell, R. E., Steinbach, P. A., Giepmans, B. N., Palmer, A. E., and Tsien, R. Y. (2004). Improved monomeric red, orange and yellow fluorescent proteins derived from *Discosoma* sp. red fluorescent protein. Nat. Biotechnol. *22*, 1567–1572.

Suh, C., Stull, N., Fujii, Y., Grinstein, S., Yaffe, M., Atkinson, S., and Dinauer, M. C. (2004). Role for p40phox in Fcgamma-receptor-induced NADPH oxidase activation. Blood *104*, 188a.

Suh, C. I., Stull, N. D., Li, X. J., Tian, W., Price, M. O., Grinstein, S., Yaffe, M. B., Atkinson, S., and Dinauer, M. C. (2006). The phosphoinositide-binding protein p40phox activates the NADPH oxidase during FcgammaIIA receptor-induced phagocytosis. J. Exp. Med. *203*, 1915–1925.

Sumimoto, H., Hata, K., Mizuki, K., Ito, T., Kage, Y., Sakaki, Y., Fukumaki, Y., Nakamura, M., and Takeshige, K. (1996). Assembly and activation of the phagocyte NADPH oxidase. Specific interaction of the N-terminal Src homology 3 domain of p47phox with p22phox is required for activation of the NADPH oxidase. J. Biol. Chem. *271*, 22152–22158.

Tian, W., Li, X. J., Stull, N. D., Ming, W., Suh, C. I., Bissonnette, S. A., Yaffe, M. B., Grinstein, S., Atkinson, S. J., and Dinauer, M. C. (2008). Fc{gamma}R-stimulated activation of the NADPH oxidase: phosphoinositide-binding protein p40phox regulates NADPH oxidase activity after enzyme assembly on the phagosome. Blood *112*, 3867–3877.

Ueyama, T., Tatsuno, T., Kawasaki, T., Tsujibe, S., Shirai, Y., Sumimoto, H., Leto, T. L., and Saito, N. (2007). A regulated adaptor function of p40phox: distinct p67phox membrane targeting by p40phox and by p47phox. Mol. Biol. Cell *18*, 441–454.

van Bruggen, R., Anthony, E., Fernandez-Borja, M., and Roos, D. (2004). Continuous translocation of Rac2 and the NADPH oxidase component p67(phox) during phagocytosis. J. Biol. Chem. *279*, 9097–9102.

Vieira, O. V., Botelho, R. J., Rameh, L., Brachmann, S. M., Matsuo, T., Davidson, H. W., Schreiber, A., Backer, J. M., Cantley, L. C., and Grinstein, S. (2001). Distinct roles of class I and class III phosphatidylinositol 3-kinases in phagosome formation and maturation. J. Cell Biol. *155*, 19–25.

Vignais, P. V. (2002). The superoxide-generating NADPH oxidase: structural aspects and activation mechanism. Cell Mol. Life Sci. *59*, 1428–1459.

Zhen, L., King, A. A., Xiao, Y., Chanock, S. J., Orkin, S. H., and Dinauer, M. C. (1993). Gene targeting of X chromosome-linked chronic granulomatous disease locus in a human myeloid leukemia cell line and rescue by expression of recombinant gp91phox. Proc. Natl. Acad. Sci. USA *90*, 9832–9836.